

Kinetic equations for thermal degradation of polymers

Aleksey D. Drozdov*

Department of Chemical Engineering

West Virginia University

P.O. Box 6102

Morgantown, WV 26506, USA

Abstract

Kinetic equations are analyzed for thermal degradation of polymers. The governing relations are based on the fragmentation–annihilation concept. Explicit solutions to these equations are derived in two particular cases of interest. For arbitrary values of adjustable parameters, the evolution of the number-average and mass-average molecular weights of polymers is analyzed numerically. Good agreement is demonstrated between the results of numerical simulation and experimental data. It is revealed that the model can correctly predict observations in thermo-gravimetric tests when its parameters are determined by matching experimental data for the decrease in molecular weight with exposure time.

PACS: 02.60.Nm; 82.35.-x; 82.30.Lp

Key-words: Polymers, Thermal degradation, Kinetic equations, Fragmentation–annihilation, Molecular weight

*E-mail: Aleksey.Drozdov@mail.wvu.edu

1 Introduction

This paper is concerned with the kinetics of thermal degradation of polymers. This subject has attracted substantial attention in the past half a century both among the specialist in theoretical physics and chemical engineering [1, 2]. This may be explained by two reasons: (i) scission (fragmentation) of macromolecules driven by thermal fluctuations at elevated temperatures provides a good example for the analysis of population dynamics in complex systems, and (ii) analysis of the degradation process becomes more and more important due to an increase in the range of temperatures for engineering applications, recycling of post-consumer plastic waste, as well as the use of polymers as biological implants and matrices for drug delivery, where depolymerization is an inevitable process affecting the life-time of an article.

Although the fact that binary scission of chains is the main mechanism for thermal degradation of polymers is widely accepted, the applicability of the fragmentation concept to the analysis of experimental data is rather limited. This may be attributed to the fact that kinetic equations for the “linear” fragmentation process involve only one adjustable parameter [3], the number too small to provide a reasonable approximation for observations. The latter implies that generalizations of conventional equations for the kinetics of fragmentation become a meaningful subject for investigation.

The following ways for “refinement” of the fragmentation concept may be mentioned:

1. An account for the influence of chains’ length and inhomogeneity of chains (the fact that the probability of a breakage event depends on the position of a bond along the backbone of a chain) on the rate of scission [4, 5, 6, 7, 8, 9].
2. An introduction of two kinds of macromolecules in a network (with strong and weak bonds) that have different rates of fragmentation [10, 11, 12].
3. An increase in the number of species in the population balance laws by accounting for interactions between chains and free radicals and the effect of the concentration of free radicals on the scission rate [13, 14, 15, 16, 17, 18].

Although these approaches seem rather attractive from the theoretical viewpoint, they are grounded on physical assumptions that are hard to be verified in experiments, on the one hand, and they result in overcomplicated explicit solutions (when the latter can be developed), on the other.

Another way to make the fragmentation concept more flexible for matching observations is to take into account some physical processes at the micro-level that accompany thermally-induced scission of macromolecules. Two candidates for this role appear to be natural: (i) aggregation (recombination) of broken chains [19, 20, 21, 22], and (ii) annihilation of fragmentation products (either in the form of creation of inert species that do not take part in further fragmentation [23, 24, 25] or as diffusion of small-size fragmentation products and their subsequent evaporation through the surface of a specimen [26, 27, 28, 29]).

In this study, we adopt the latter approach and accept the conventional hypothesis that the diffusivity of detached end- and side-groups at the degradation temperature is so large that the kinetics of diffusion may be disregarded. This allows the number of adjustable parameters in the governing equations to be reduced to four, the number that gives an opportunity to analyze the influence of all these quantities on the evolution of molecular weight of polymers.

Analysis of the effect of diffusivity of oligomers on the degradation kinetics will be the subject of a subsequent paper.

Unlike previous studies, which focused mainly on the scaling solutions to the fragmentation–annihilation equations (the latter provide valuable information about the properties of the degradation process at small and large times), we concentrate on the kinetics of polymer degradation within the time-scale of conventional tests. Another difference between the present work and previous publications is that we deal with changes in the number-average and mass-average molecular weights, the standard quantities measured in experiments. This allows our analytical and numerical results to be compared with available observations.

The objective of this study is two-fold:

- To report some analytical and numerical solutions to the fragmentation–annihilation equations.
- To establish restrictions on the material constants in the governing relations imposed by the time–temperature and time–molecular weight superposition principles, and to find adjustable parameters in the kinetic equations by matching observations.

We believe that the knowledge of these quantities (or, at least, their orders of magnitude and mutual relations between different constants) may be helpful for further analytical and numerical investigation of the degradation process.

In fitting experimental data, we concentrate on thermal degradation of polystyrene (PS), poly(α -methylstyrene) (PAMS) and poly(L-lactide) (PLLA). The choice of these polymers may be explained by their wide use in industrial applications, including food service packaging (PS and PAMS) and scaffolds for transplanted organs (PLLA), the areas, where the degradation process is of the highest importance. Another (merely technical) reason for this choice is that observations are available on these polymers with low polydispersity indices (less than two), which implies that no additional parameters associated with the initial distribution of chains should be introduced into the model.

The paper is organized as follows. We begin with the formulation of kinetic equations in Section 2. Some explicit solutions to these equations are derived in Section 3. The effect of material constants on the evolution of molecular weight of polymers subjected to thermal degradation is studied numerically in Section 4. The time–molecular weight and time–temperature superposition principles are discussed in Sections 5 and 6, respectively. In Section 7, we demonstrate that the model can adequately predict observations in thermo-gravimetric tests. Some concluding remarks are formulated in Section 8.

2 Kinetic equations

In this section, kinetic equations are formulated for the analysis of thermal degradation of polymers based on the fragmentation–annihilation concept.

2.1 Binary scission of chains

Denote by $\bar{N}(t)$ the number of macromolecules per unit mass of a polymer network at an arbitrary instant $t \geq 0$. Following common practice, we treat chains as sequences of segments

connected by bonds. Each chain in the network is entirely characterized by the numbers of segments k ($k = 1, 2, \dots$). Denote by $N_k(t)$ is the number of chains (per unit mass) at time t containing k segments. The functions $N_k(t)$ obey the conservation law

$$\bar{N}(t) = \sum_{k=1}^{\infty} N_k(t). \quad (1)$$

Binary scission (fragmentation) of chains is described by the reactions

$$N_k \rightarrow N_l + N_{k-l} \quad (l = 1, \dots, k-1).$$

Denote by γ the rate of scission (the number of scission events per bond between segments per unit time). Assuming $\gamma = \gamma_0$ to be independent of the number of segments k , we arrive at the kinetic equations for the functions $N_k(t)$

$$\frac{dN_k}{dt}(t) = -\gamma_0(k-1)N_k(t) + 2\gamma_0 \sum_{j=k+1}^{\infty} N_j(t). \quad (2)$$

The coefficient $k-1$ in the first term describes the number of possible scission events in a chain containing k segments. The coefficient “2” before the sum in Eq. (2) indicates that there are two opportunities (“left” and “right”) to obtain a chain with k segments after scission of a macromolecule with a larger number of segments.

Equation (2) can be easily generalized by assuming the rate of scission γ to be a function of chains’ length. Conventionally, the power-law dependence is adopted to account for this dependence

$$\gamma(k) = \gamma_0 k^a, \quad (3)$$

where γ_0 and a are material parameters. The kinetic equations for fragmentation of chains with the length-dependent rate of scission (3) read

$$\frac{dN_k}{dt}(t) = -\gamma_0 k^a(k-1)N_k(t) + 2\gamma_0 \sum_{j=k+1}^{\infty} j^a N_j(t). \quad (4)$$

2.2 Annihilation of chains

Thermal fluctuations in a network induce not only binary scission of macromolecules, but also detachment of end- and side-groups from polymer chains. As these groups are rather small, they have relatively large diffusivity and can easily leave a specimen. A decrease in a sample’s mass with time driven by separation of end- and side-groups and their desorption is treated as their annihilation.

To make the model tractable from the mathematical standpoint, we suppose that detachment of small groups within the interval $[t, t + dt]$ may be thought of as transformation of a chain with k segments into a chain with $k-1$ segment. Denote by Γ the ratio of the number of chains that lose a segment per unit time to the entire number of chains. Assuming the annihilation rate to grow with the number of segments in a chain following the power law similar to Eq. (3),

$$\Gamma(k) = \Gamma_0 k^b, \quad (5)$$

where Γ_0 and b are material parameters, we arrive at the kinetic equations

$$\frac{dN_k}{dt}(t) = -\gamma_0 k^a (k-1)N_k(t) + 2\gamma_0 \sum_{j=k+1}^{\infty} j^a N_j(t) + \Gamma_0 [(k+1)^b N_{k+1}(t) - k^b N_k(t)]. \quad (6)$$

The number-average molecular weight M_n and the mass-average molecular weight M_w of a polymer read

$$M_n(t) = \frac{\sum_{k=1}^{\infty} k N_k(t)}{\sum_{k=1}^{\infty} N_k(t)}, \quad M_w(t) = \frac{\sum_{k=1}^{\infty} k^2 N_k(t)}{\sum_{k=1}^{\infty} k N_k(t)}. \quad (7)$$

The objective of this work is to analyze changes in $M_n(t)$ and $M_w(t)$ with time t , when the functions $N_k(t)$ are governed by Eq. (6).

2.3 Transformation of the kinetic equations

Introducing the concentrations of chains with k segments,

$$n_k(t) = \frac{N_k(t)}{N_0}, \quad (8)$$

where $\bar{N}_0 = \bar{N}(0)$ is the total number of chains at the initial instant $t = 0$, we present Eq. (6) in the form

$$\frac{dn_k}{dt}(t) = -\gamma_0 k^a (k-1)n_k(t) + 2\gamma_0 \sum_{j=k+1}^{\infty} j^a n_j(t) + \Gamma_0 [(k+1)^b n_{k+1}(t) - k^b n_k(t)]. \quad (9)$$

Following common practice, it is convenient to suppose that the number of segments in a chain is large compared to unity and to replace the discrete index k in Eq. (9) by a continuous argument x . This results in the integro-differential equation for the function $n(t, x)$

$$\frac{\partial n}{\partial t}(t, x) = -\gamma_0 x^{a+1} n(t, x) + 2\gamma_0 \int_x^{\infty} y^a n(t, y) dy + \Gamma_0 \frac{\partial}{\partial x} (x^b n(t, x)). \quad (10)$$

The initial condition for Eq. (10) reads

$$n(0, x) = n_0(x), \quad (11)$$

where $n_0(x)$ is a given function. We do not formulate boundary conditions for the function $n(t, x)$, but assume that this function does not grow very strongly at $x = 0$ and decays rapidly at $x \rightarrow \infty$ in the sense that the integrals M_m exist,

$$M_m(t) = \int_0^{\infty} x^m n(t, x) dx \quad (m = 0, 1, 2, \dots). \quad (12)$$

3 Explicit solutions

At $\Gamma_0 = 0$, i.e. when the annihilation process is suppressed, an analytical solution of Eq. (10) was found in [5] for an arbitrary integer $a \geq 0$. However, an appropriate solution for $a > 0$ is so complicated that it can say practically nothing about the behavior of the function $n(t, x)$

and its moments $M_m(t)$. This implies that we confine ourselves to the case $a = 0$ in the search for explicit solutions of Eq. (10). Following [5], we assume the parameter b in Eq. (10) to be an integer as well, $b = l$ ($l = 1, 2, \dots$), and re-write Eq. (10) in the form

$$\frac{\partial n}{\partial t}(t, x) = -\gamma_0 n(t, x) + 2\gamma_0 \int_x^\infty n(t, y) dy + \Gamma_0 \frac{\partial}{\partial x} (x^l n(t, x)). \quad (13)$$

Integrating Eq. (13) over x^m ($m = 0, 1, \dots$) and using notation (12), we find that

$$\frac{dM_m}{dt}(t) = -\gamma_0 M_{m+1}(t) + 2\gamma_0 \int_0^\infty x^m dx \int_x^\infty n(t, y) dy + \Gamma_0 \int_0^\infty x^m \frac{\partial}{\partial x} (x^l n(t, x)) dx. \quad (14)$$

The first integral in Eq. (14) is transformed by changing the order of integration,

$$\int_0^\infty x^m dx \int_x^\infty n(t, y) dy = \int_0^\infty n(t, y) dy \int_0^y x^m dx = \frac{1}{m+1} \int_0^\infty y^{m+1} n(t, y) dy = \frac{1}{m+1} M_{m+1}(t).$$

The other integral is calculated by integration by parts,

$$\int_0^\infty x^m \frac{\partial}{\partial x} (x^l n(t, x)) dx = -m \int_0^\infty x^{m+l-1} n(t, x) dx = -m M_{m+l-1}(t).$$

Substitution of these expressions into Eq. (14) results in the differential equation

$$\frac{dM_m}{dt}(t) = -\gamma_0 \left(1 - \frac{2}{m+1}\right) M_{m+1}(t) - \Gamma_0 m M_{m+l-1}(t). \quad (15)$$

Our purpose now is to find explicit solutions of Eq. (15) for $l = 1$ and $l = 2$. According to Eq. (5), the former case corresponds to scission and annihilation of end-groups exclusively, whereas the latter case describes annihilation of side-groups homogeneously distributed along a chain's backbone.

3.1 The case $l = 1$

Setting $l = 1$ in Eq. (15), we obtain

$$\frac{dM_m}{dt}(t) = -\Gamma_0 m M_m(t) - \gamma_0 \left(1 - \frac{2}{m+1}\right) M_{m+1}(t). \quad (16)$$

Introducing the notation

$$T_m(\tau) = M_m(t) \exp(\Gamma_0 m t), \quad \tau = \int_0^t \exp(-\Gamma_0 s) ds, \quad (17)$$

we transform Eq. (16) as follows:

$$\frac{dT_m}{d\tau}(\tau) = -\gamma_0 \left(1 - \frac{2}{m+1}\right) T_{m+1}(\tau). \quad (18)$$

Comparison of Eqs. (15) and (18) implies that in the special case $l = 1$, the kinetics of the fragmentation–annihilation process coincides with the kinetics of a mere fragmentation process

in the new time τ for the new moments T_m . In particular, putting $m = 0$ and $m = 1$ in Eq. (18), we find that

$$\frac{dT_0}{d\tau} = \gamma_0 T_1, \quad \frac{dT_1}{d\tau} = 0.$$

The solutions of these equations are given by

$$T_0(\tau) = T_0(0) + \gamma_0 T_1(0)\tau, \quad T_1(\tau) = T_1(0). \quad (19)$$

The moment $T_2(\tau)$ is determined by the formula

$$T_2(\tau) = \frac{2}{(\gamma_0\tau)^2} \left[\hat{n}_0(\gamma_0\tau) - T_0(0) + T_1(0)\gamma_0\tau \right], \quad (20)$$

where $\hat{n}_0(z)$ is the Laplace transform of the function $n_0(x)$. A detailed derivation of Eq. (20) is given in Appendix. It follows from Eqs. (17), (19) and (20) that

$$\begin{aligned} M_0(t) &= \left[M_0(0) + M_1(0) \frac{\gamma_0}{\Gamma_0} (1 - \exp(-\Gamma_0 t)) \right], \\ M_1(t) &= M_1(0) \exp(-\Gamma_0 t), \\ M_2(t) &= 2 \left(\frac{\Gamma_0}{\gamma_0} \right)^2 \frac{\exp(-2\Gamma_0 t)}{(1 - \exp(-\Gamma_0 t))^2} \left[\hat{n}_0 \left(\frac{\gamma_0}{\Gamma_0} (1 - \exp(-\Gamma_0 t)) \right) \right. \\ &\quad \left. - M_0(0) + M_1(0) \frac{\gamma_0}{\Gamma_0} (1 - \exp(-\Gamma_0 t)) \right]. \end{aligned} \quad (21)$$

Substituting Eq. (21) into Eq. (7), where the sums are replaced by integrals, we arrive at explicit expressions for the number-average and mass-average molecular weights as functions of time t .

3.2 The case $l = 2$

Setting $l = 2$ in Eq. (15), we obtain

$$\frac{dM_m}{dt}(t) = -\gamma_0 \left(\frac{m-1}{m+1} + \frac{\Gamma_0}{\gamma_0} m \right) M_{m+1}(t). \quad (22)$$

Assuming the initial network of chains to be monodisperse,

$$n_0(x) = \delta(x - L), \quad (23)$$

where L is the initial length of chains, we solve Eq. (22) by Charlesby's method [30]. As Eq. (22) is linear with respect to the unknown function $n(t, x)$, appropriate formulas for the moments $M_m(t)$ corresponding to an arbitrary initial condition $n_0(x)$ are developed by the superposition method.

The m th moment $M_m(t)$ is expanded into the Taylor series in time,

$$M_m(t) = \sum_{k=0}^{\infty} \frac{M^{(k)}(0)}{k!} t^k, \quad (24)$$

where $M_m^{(k)}(0)$ stands for the k th derivative at the point $t = 0$. Substitution of Eq. (24) into Eq. (22) implies that for an arbitrary $k > 1$,

$$M_m^{(k)}(0) = (-\gamma_0)^k \prod_{j=0}^{k-1} \left(\frac{m+j-1}{m+j+1} + \frac{\Gamma_0}{\gamma_0}(m+j) \right) M_{m+k}(0). \quad (25)$$

It follows from Eqs. (12) and (23) that

$$M_m(0) = L^m. \quad (26)$$

Substitution of expressions (25) and (26) into Eq. (24) results in

$$M_m(t) = L^m \left[1 + \sum_{k=1}^{\infty} A_{mk} (-\gamma_0 t L)^k \right], \quad (27)$$

where

$$A_{mk} = \frac{1}{k!} \prod_{j=0}^{k-1} \left(\frac{m+j-1}{m+j+1} + \frac{\Gamma_0}{\gamma_0}(m+j) \right).$$

Introducing the new variable $j' = j + 1$ and omitting the prime, we obtain

$$A_{mk} = \prod_{j=1}^k \frac{1}{j} \left(\frac{m+j-2}{m+j} + \frac{\Gamma_0}{\gamma_0}(m+j-1) \right). \quad (28)$$

It follows from Eq. (27) that for an arbitrary initial condition $n_0(x)$, the moments $M_m(t)$ are given by

$$\begin{aligned} M_m(t) &= \int_0^{\infty} n_0(x) x^m \left[1 + \sum_{k=1}^{\infty} A_{mk} (-\gamma_0 t x)^k \right] dx \\ &= M_m(0) + \sum_{k=1}^{\infty} A_{mk} M_{m+k}(0) (-\gamma_0 t)^k. \end{aligned} \quad (29)$$

Although Eq. (29) provides explicit expressions for the moments $M_m(t)$, it is not rather convenient for the numerical analysis, because the series converges slowly. Formulas (28) and (29) are helpful, however, for the evaluation of changes in $M_m(t)$ at small times, when $\gamma_0 t \ll 1$. Neglecting terms beyond the first order of smallness in Eq. (29), we find that

$$\begin{aligned} M_0(t) &= M_0(0) + M_1(0) \gamma_0 t, & M_1(t) &= M_1(0) - M_2(0) \Gamma_0 t, \\ M_2(t) &= M_2(0) - M_3(0) \left(\frac{\gamma_0}{3} + 2\Gamma_0 \right) t. \end{aligned} \quad (30)$$

According to Eq. (30), changes in the moments $M_0(t)$ and $M_1(t)$ are governed by two different processes: an increase in $M_0(t)$ is driven by fragmentation of chains, whereas a decrease in $M_1(t)$ is induced by annihilation of end- and side-groups. Introducing the notation

$$d(t) = \frac{M_1(t)}{M_1(0)}, \quad d_n(t) = \frac{M_n(t)}{M_n(0)}, \quad d_w(t) = \frac{M_w(t)}{M_w(0)} \quad (31)$$

and using Eq. (7), we present Eq. (30) in the form

$$\begin{aligned} d(t) &= 1 - M_w(0) \Gamma_0 t, & d_n(t) &= 1 - (M_n(0) \gamma_0 + M_w(0) \Gamma_0) t, \\ d_w(t) &= 1 - \left[M_w(0) \Gamma_0 + M_z(0) \left(\frac{\gamma_0}{3} + 2\Gamma_0 \right) \right] t, \end{aligned} \quad (32)$$

where the conventional notation is used $M_z(t) = M_3(t)/M_2(t)$.

4 Numerical analysis

As explicit formulas for the moments $M_m(t)$ can be derived only for a limited set of values of the exponents a and b , it is of interest to analyze the evolution of M_m with time t numerically for arbitrary values of these parameters. For this purpose, we integrate Eq. (9) numerically with the initial condition

$$n_k(0) = \delta_{kK}, \quad (33)$$

where δ_{ij} denotes the Kronecker delta. Equation (33) corresponds to the monodisperse distribution of chains that contain K segments at the initial instant $t = 0$. To reduce the number of material parameters, we introduce the dimensionless time $t' = \gamma_0 t$ and set

$$\eta = \frac{\Gamma_0}{\gamma_0}. \quad (34)$$

In the new notation, Eq. (9) reads (the prime is omitted for simplicity)

$$\frac{dn_k}{dt}(t) = -k^a(k-1)n_k(t) + 2 \sum_{j=k+1}^K j^a n_j(t) + \eta \left[(k+1)^b n_{k+1}(t) - k^b n_k(t) \right] \quad (k = 1, 2, \dots, K). \quad (35)$$

The limitation on the number of equations in Eq. (35) follows from the fact that if the maximal number of segments in a chain equals K at $t = 0$, no chains with higher number of segments can appear at $t > 0$ due to the fragmentation–annihilation process. Equations (33) and (35) involve four material constants: a , b , η and K . In the numerical simulation, we fix $K = 100$ and study the effect of other parameters on the number-average and mass-average molecular weights determined by Eqs. (7) and (8). Integration of Eq. (35) is performed by the Runge–Kutta method with the step $\Delta t = 1.0 \cdot 10^{-6}$.

First, we set $a = 0$ and $b = 1$ and study the effect of η on the ratios $d_n(t)$ and $d_w(t)$ defined by Eq. (31). Figures 1 and 2 demonstrate that annihilation of end- and side-groups affects the degradation process noticeably when the rate of annihilation Γ_0 exceeds the rate of scission γ_0 by an order of magnitude.

Afterwards, we fix $\eta = 10.0$, $b = 1.0$ and analyze the influence of the exponent a on the dimensionless ratios d_n and d_w . Figures 3 and 4 reveal that an increase in a results in a very strong decrease in d_n and d_w for any $t > 0$. When $a \approx 1$, the curves $d_n(t)$ and $d_w(t)$ steeply drop at small times and remain practically constant at larger times. These results make questionable the applicability of the analytical solution developed in [5] (this solution corresponds to $a = 2$) for the description of the degradation process.

Finally, we fix $a = 0.2$, $\eta = 10.0$ and assess the effect of the exponent b on $d_n(t)$ and $d_w(t)$. Figures 5 and 6 show that the influence of b is negligible when $b \in [0, 1)$. However, for $b > 1$, the effect of this parameter becomes substantial, and an increase in b causes a pronounced decrease in number-average and mass-average molecular weights.

To ensure the accuracy of numerical simulation, we use three tests. First, we verify that at $\eta = 0$, the first moment M_1 remains independent of time [this conclusion follows from Eq. (15), where we set $\Gamma_0 = 0$]. Secondly, we increase K by twice, decrease the rate of fragmentation γ_0 by twice and check that the moments $M_n(t)$ and $M_w(t)$ remain unchanged. The latter implies that the results of numerical analysis are independent of our choice of $K = 100$. Finally, we perform simulation with $a = 0$ and $b = 1$ and confirm that the numerical results for the moments $M_m(t)$ ($m = 0, 1, 2$) coincide with analytical solution (21).

5 Time–molecular weight superposition principle

Experimental data for monodisperse polymers reveal that observations for the ratios of number-average and mass-average molecular weights, $d_n(t)$ and $d_w(t)$, obtained at various initial molecular weights and plotted in semi-logarithmic coordinates (versus the logarithm of time) may be superposed (with an acceptable level of accuracy) by shifts along the time axis. The construction of a master-curve by shift of creep and relaxation curves measured at various temperatures is a conventional procedure in linear viscoelasticity of polymers [31]. The validity of this operation is based on the time–temperature superposition principle, which asserts that only the characteristic creep and relaxation times are affected by temperature, while other parameters (elastic moduli and shapes of the relaxation spectra) remain temperature-independent. Our aim now is to establish an analogous principle for the effect of initial molecular weight of monodisperse polymers on the fragmentation–annihilation process. For this purpose, we return to integro-differential equation (10) and introduce the dimensionless variables

$$t_* = \frac{t}{\Theta}, \quad x_* = \frac{x}{L}, \quad (36)$$

where Θ is the characteristic time for degradation. In the new notation, Eq. (10) reads

$$\frac{\partial n}{\partial t_*}(t_*, x_*) = \gamma_0 \Theta L^{a+1} \left[-x_*^{a+1} n(t_*, x_*) + 2 \int_{x_*}^{\infty} y_*^a n(t_*, y_*) dy_* + \eta L^{b-a-2} \frac{\partial}{\partial x_*} (x_*^b n(t_*, x_*)) \right]. \quad (37)$$

It follows Eq. (37) that any solution $n(t_*, x_*)$ is independent of the initial molecular weight L [this statement implies the time–molecular weight superposition principle] provided that

$$b = a + 2. \quad (38)$$

Under condition (38), the shift factor $A = \Theta/\Theta^{\text{ref}}$, where Θ^{ref} is the characteristic time corresponding to a reference molecular weight L^{ref} , is determined by the formula

$$\log A = (a + 1) \log \frac{L}{L^{\text{ref}}} \quad (39)$$

with $\log = \log_{10}$. According to the time–molecular weight superposition principle, the number of adjustable parameters in the model may be substantially reduced: instead of four material constants, γ_0 , Γ_0 , a and b , we have only two parameters to be found, γ_0 and η : the exponent a is uniquely determined from Eq. (39), whereas the exponent b is given by Eq. (38).

5.1 Fitting of observations on polystyrene

To find the values of γ_0 and η and to assess the influence of annihilation of end- and side-groups on the degradation process, we focus on observations reported by Madras et al. [11] on thermal degradation of monodisperse PS in a mineral oil at the temperature $T = 275^\circ\text{C}$. For a detailed description of specimens and the experimental procedure, the reader is referred to [11]. The ratio d_w of mass-average molecular weights is depicted versus exposure time t in Figure 7. The experimental data for $M_w(0) = 26$ kg/mol are presented without changes. Observations for the other initial molecular weights ($M_w(0) = 12, 110, 210, 330$ and 930 kg/mol) are shifted

along the time-axis by appropriate amounts A that are determined from the condition that all available data produce a smooth master-curve.

The parameter A is plotted versus the ratio of initial molecular weights $M_w(0)/M_w^{\text{ref}}(0)$ with $M_w^{\text{ref}}(0) = 26$ kg/mol in Figure 8. The experimental data are approximated by the function

$$\log A = A_0 + A_1 \log \frac{M_w(0)}{M_w^{\text{ref}}(0)}, \quad (40)$$

where the coefficients A_k ($k = 0, 1$) are determined by the least-squares method. Figure 8 demonstrates that Eq. (40) provides good matching of the observations with $A_0 \approx 0$ and $A_1 \approx 1$. With reference to this result, we conclude from Eqs. (38), (39) and (40) that one should set $a = 0$ and $b = 2$ in Eq. (35) in order to reproduce the experimental data plotted in Figure 7.

The fact that $A_1 \approx 1$, which implies that the fragmentation rate γ_0 is proportional to the initial mass-average molecular weight $M_w(0)$,

$$\frac{\gamma_0}{\gamma_0^{\text{ref}}} = \frac{M_w(0)}{M_w^{\text{ref}}(0)}, \quad (41)$$

has been revealed about 40 years ago [32]. It was also shown that Eq. (41) is valid when the initial molecular weight $M_w(0)$ is not very large: for polymers with ultra-high molecular weights, the fragmentation rate γ_0 grows like the square-root of the molecular weight [33].

To find γ_0 and η , we fix some intervals $[0, \gamma_{\text{max}}]$ and $[0, \eta_{\text{max}}]$, where the “best-fit” parameters γ_0 and η are assumed to be located, and divide these intervals into J subintervals by the points $\gamma^{(i)} = i\Delta\gamma$, and $\eta^{(j)} = j\Delta\eta$ ($i, j = 1, \dots, J-1$) with $\Delta\gamma = \gamma_{\text{max}}/J$ and $\Delta\eta = \eta_{\text{max}}/J$. For any pair $\{\gamma^{(i)}, \eta^{(j)}\}$, Eq. (35) with initial condition (33) is integrated numerically by the Runge–Kutta method with $K = 100$ and the time-step $\Delta t = 0.1$. This, relatively large, step is chosen because the fragmentation rates under consideration γ_0 are quite small (of order of 10^{-5}). The best-fit parameters γ_0 and η are determined from the condition of minimum of the function

$$R = \sum_{t_m} \left[d_w^{\text{exp}}(t_m) - d_w^{\text{num}}(t_m) \right]^2,$$

where the sum is calculated over all times t_m at which observations are presented in Figure 7, d_w^{exp} is the ratio of mass-average molecular weights measured in the tests, and d_w^{num} is given by Eqs. (7), (8) and (31). Figure 7 demonstrates fair agreement between the observations at various initial molecular weights and the results of numerical simulation with $\gamma_0 = 1.4 \cdot 10^{-5}$ and $\eta = 1.0$. Two conclusions may be drawn from the numerical analysis: (i) the model correctly describes the experimental data, and (ii) the best-fit value $\eta = 1.0$ found by matching the observations on monodisperse polystyrene results in a rather weak influence of the annihilation process on the kinetics of thermal degradation (see Figures 1 and 2). Our purpose now is to demonstrate that this is not the case for other polymers. To show that annihilation of end- and side-groups noticeably affects the degradation process, we analyze two sets of observations on PAMS and PLLA obtained at various temperatures T .

6 Time–temperature superposition principle

We begin with the discussion of the effect of temperature T on the kinetics of thermal degradation. To establish conditions on the material constants which ensure that the time–temperature

superposition principle holds for the ratios d_n and d_w , i.e. that the functions $d_n(t)$ and $d_w(t)$ measured at various temperatures and plotted in semi-logarithmic coordinates may be shifted along the time-axis to construct a master-curve [10], we return to the dimensionless integro-differential equation (37).

According to the Eyring theory [34], the effect of temperature on the rates of thermally activated processes may be accounted for by the formulas

$$\gamma_0 = \gamma_0^{\text{ref}} \exp\left[-\frac{E_\gamma}{R}\left(\frac{1}{T} - \frac{1}{T^{\text{ref}}}\right)\right], \quad \Gamma_0 = \Gamma_0^{\text{ref}} \exp\left[-\frac{E_\Gamma}{R}\left(\frac{1}{T} - \frac{1}{T^{\text{ref}}}\right)\right], \quad (42)$$

where T is the absolute temperature, R is the universal gas constant, E_γ and E_Γ are appropriate activation energies, and γ_0^{ref} and Γ_0^{ref} are rates of fragmentation and annihilation at the reference temperature T^{ref} . Equation (37) implies that the time-temperature superposition principle is valid, provided that the exponents a and b are independent of temperature, while the rates of fragmentation and annihilation, γ_0 and Γ_0 , are affected by T in a similar fashion,

$$a = a^{\text{ref}}, \quad b = b^{\text{ref}}, \quad E_\gamma = E_\Gamma = E. \quad (43)$$

The first two conditions in Eq. (43) seem quite natural, whereas the last equality imposes rather strong restrictions on the degradation process. In what follows, it will be shown that the latter condition is fulfilled for some polymers and is violated for others.

6.1 Fitting of observations on poly(α -methylstyrene)

We begin with the analysis of observations for thermo-oxidative degradation on PAMS with the initial mass-average molecular weight $M_w(0) = 9.0$ kg/mol and the polydispersity index $D = 2$ reported by Sterling et al. [16]. These data demonstrate that the time-temperature superposition principle is satisfied for the degradation process with a high level of accuracy.

In each test, a specimen was dissolved in 1,2,4-trichlorobenzene, heated to a fixed reaction temperature T in the range from 110 to 150 °C, and di-tert-butyl peroxide was added to a reaction vessel with a constant flow rate under stirring. Specimens for GPC (gel permeation chromatography) analysis were taken every 45 min. For a detailed description of the experimental procedure, see [16].

Changes in the ratio of number-average molecular weights d_n with time t are depicted in Figure 9. The experimental data at $T^{\text{ref}} = 110$ °C are presented without changes. Observations at the other temperatures ($T = 120, 130, 140$ and 150 °C) are shifted along the time-axis by appropriate amounts A that are determined from the condition that the experimental data produce a smooth master-curve.

The parameter A is plotted in Figure 10 versus temperature T . The experimental data are approximated by the dependence [that follows from Eq. (42)]

$$\ln A = A_0 - \frac{A_1}{T} \quad (44)$$

with

$$A = \frac{\gamma_0}{\gamma_0^{\text{ref}}}, \quad A_0 = \frac{E}{RT^{\text{ref}}}, \quad A_1 = \frac{E}{R}. \quad (45)$$

The coefficients A_k ($k = 0, 1$) in Eq. (44) are determined by the least-squares method. Figure 10 demonstrates that Eq. (44) ensures quite acceptable fit of the observations. According to Eq. (45) and Figure 10, the activation energy reads $E = 86$ kJ/mol. This value is in reasonable agreement with the activation energy $E = 112$ kJ/mol found by Brown and Wall [33] by applying a graphic method (whose accuracy is rather low due to the numerical estimation of derivatives) and in excellent accord with the activation energies recently determined for other polymers by using more sophisticated techniques ($E = 88$ kJ/mol for low-density polyethylene [12] and $E = 98$ kJ/mol for polypropylene [10]).

To reduce the number of adjustable parameters in Eq. (35), we set $a = 0$, which means that we presume the rate of fragmentation to be independent of chains' length. To find the quantities γ_0 , b and η , we use an algorithm similar to that employed in Section 5. We fix some intervals $[0, \gamma_{\max}]$, $[0, b_{\max}]$ and $[0, \eta_{\max}]$, where the "best-fit" parameters γ_0 , b and η are assumed to be located, and divide these intervals into J subintervals by the points $\gamma^{(i)} = i\Delta\gamma$, $b^{(j)} = j\Delta b$ and $\eta^{(k)} = k\Delta\eta$ ($i, j, k = 1, \dots, J - 1$) with $\Delta\gamma = \gamma_{\max}/J$, $\Delta b = b_{\max}/J$ and $\Delta\eta = \eta_{\max}/J$. For any triple $\{\gamma^{(i)}, b^{(j)}, \eta^{(k)}\}$, Eq. (35) with initial condition (33) is integrated numerically by the Runge-Kutta method with $K = 100$ and the time-step $\Delta t = 0.1$. The best-fit parameters γ_0 , b and η are determined from the condition of minimum of the function

$$R = \sum_{t_m} \left[d_n^{\text{exp}}(t_m) - d_n^{\text{num}}(t_m) \right]^2, \quad (46)$$

where the sum is calculated over all times t_m at which observations are presented in Figure 9, d_n^{exp} is the ratio of number-average molecular weights measured in the tests, and d_n^{num} is given by Eqs. (7), (8) and (31). Figure 9 demonstrates good agreement between the observations at various temperatures T and the results of numerical simulation with $\gamma_0 = 9.0 \cdot 10^{-7}$, $b = 1.5$ and $\eta = 50.0$.

As the value of η is rather large compared to unity, we draw a conclusion from Figures 1, 2 and 9 that the effect of annihilation of end- and side-groups on the degradation kinetics of PAMS is substantial. The observation that the rate of annihilation for PAMS ($\eta = 50$) exceeds that for PS ($\eta = 1$) by about two orders of magnitude appears to be natural, because PAMS chains differ from those of PS by the presence of methyl groups attached to each tertiary backbone carbon [16].

6.2 Fitting of observations on poly(*L*-lactide)

We proceed with the analysis of experimental data on thermal degradation of PLLA reported by Yu et al. [22]. PLLA samples with the initial mass-average molecular weight $M_w(0) = 108$ kg/mol and the polydispersity index $D = 1.5$ were heated to a required temperature T (in the range between 180 to 220 °C), preserved at this temperature in a reaction vessel under nitrogen atmosphere for given amounts of time (from 0.5 to 6.0 h), subsequently removed from the vessel, and their molecular weights were measured by GPC. The ratio of the number-average molecular weights d_n is plotted versus exposure time t in Figure 11. This figure shows that the time-temperature superposition principle is not valid for the degradation process (the experimental data at $T = 200$ and $T = 220$ °C re-plotted in the semi-logarithmic scale cannot be superposed by shifts along the time-axis with an acceptable level of accuracy). This conclusion may be explained by the fact that the activation energies E_γ and E_T noticeably differ from each other.

To validate this result and to assess the difference between the activation energies for fragmentation and annihilation, we approximate each curve depicted in Figure 11 separately. To reduce the number of adjustable parameters, we set $a = 0$ (which means that the fragmentation rate is assumed to be independent of chains' length) and $b = 2.5$ (this value is taken because the observations at $T = 200$ and $T = 220$ °C depicted in Figure 11 resemble our results of numerical simulation with $b = 2.5$ reported in Figure 5). The fact that the rate of fragmentation in PLLA specimens with relatively small molecular weights (less than 300 kg/mol) is independent of chains' length is confirmed by the experimental data reported by Bywater and Black (see Figure 3 in [32]).

The rates γ_0 and Γ_0 are determined by using an algorithm similar to that described in Section 5. We fix some intervals $[0, \gamma_{\max}]$ and $[0, \Gamma_{\max}]$, where the “best-fit” parameters γ_0 and Γ_0 are assumed to be located, and divide these intervals into J subintervals by the points $\gamma^{(i)} = i\Delta\gamma$ and $\Gamma^{(j)} = j\Delta\Gamma$ ($i, j = 1, \dots, J-1$) with $\Delta\gamma = \gamma_{\max}/J$ and $\Delta\Gamma = \Gamma_{\max}/J$. For any pair $\{\gamma^{(i)}, \Gamma^{(j)}\}$, Eq. (35) with initial condition (33) is integrated numerically by the Runge–Kutta method with $K = 100$ and the time-step $\Delta t = 0.1$. The best-fit parameters γ_0 and Γ_0 are determined from the condition of minimum of the cost function (46). Figure 11 reveals good agreement between the observations at all three temperatures T under consideration and the results of numerical simulation. The ratio η determined by Eq. (34) ranges from 0.9 at $T = 180$ to 11.0 at $T = 200$ and to 15.0 at $T = 220$ °C. These values together with the results depicted in Figures 1 and 2 show that the effect of annihilation of end- and side-groups on the degradation process is quite substantial, and the influence of this process increases with temperature.

The adjustable parameters γ_0 and Γ_0 are plotted versus temperature T in Figure 12. The experimental data are approximated by the equations similar to Eq. (44),

$$\ln A = A_0 - \frac{A_1}{T}, \quad \ln B = B_0 - \frac{B_1}{T} \quad (47)$$

with $T^{\text{ref}} = 453$ K (180 °C) and

$$\begin{aligned} A &= \frac{\gamma_0}{\gamma_0^{\text{ref}}}, & A_0 &= \frac{E_\gamma}{RT^{\text{ref}}}, & A_1 &= \frac{E_\gamma}{R}, \\ B &= \frac{\Gamma_0}{\Gamma_0^{\text{ref}}}, & B_0 &= \frac{E_\Gamma}{RT^{\text{ref}}}, & B_1 &= \frac{E_\Gamma}{R}. \end{aligned} \quad (48)$$

Equations (47) follow from Eq. (42). Figure 12 shows that Eq. (47) provides an acceptable fit of the observations (it should be noted some scatter of the experimental data). However, the deviations of the data from Eq. (42) are noticeably less pronounced than the difference between curves 1 and 2 in Figure 12, which confirms our hypothesis that fragmentation and annihilation of chains may be governed by different processes at the micro-level.

The activation energy found for the fragmentation process, $E_\gamma = 91.9$ kJ/mol, is in good agreement with the value of E_γ determined for PAMS. The fact that the activation energy for annihilation of end- and side-groups ($E_\Gamma = 223.9$ kJ/mol) exceeds by about twice that for fragmentation of chains implies that the annihilation process strongly affects polymer degradation at elevated temperatures, whereas its influence is of secondary importance at relatively low temperatures. This conclusion provides a clue to explain our results of numerical simulation

on PS specimens: the temperature $T = 275$ °C is relatively low for intensive breakage of end- and side-groups in polystyrene, which implies that the value $\eta = 1.0$ found by matching the experimental data is rather small.

7 Thermo-gravimetric analysis

It was revealed in the previous sections that the model can correctly describe experimental data on the evolution of molecular weights with exposure time in conventional depolymerization tests. It should be noted, however, that other kinetic models grounded on either the fragmentation concept or the aggregation–fragmentation theory can reproduce at least some of these observations with a reasonable level of accuracy. What cannot be described by the conventional models (all of which imply the conservation law for the number of segments in a network) is observations in thermo-gravimetric experiments, where a decrease in a sample’s mass is measured as a function of exposure time at elevated temperatures.

Our aim now is to demonstrate that (i) the model grounded on the fragmentation–annihilation concept can qualitatively describe experimental data in thermo-gravimetric tests, and (ii) the kinetic equations with adjustable parameters determined by matching observations in GPC tests can quantitatively predict results of thermo-gravimetric analysis (TGA).

Two kinds of TGA tests are conventionally performed. In experiments with a constant rate of heating $q = dT/dt$, mass \bar{m} of a specimen is measured as a function of exposure time t and the ratio

$$d(t) = \frac{\bar{m}(t)}{\bar{m}(0)}$$

of the current mass $\bar{m}(t)$ to the initial mass $\bar{m}(0)$ is plotted as a function of current temperature $T(t)$. The graph $d(T)$ demonstrates the following features: (i) d remains practically constant and equal unity up to some temperature T_{onset} , at which the degradation process starts, (ii) d sharply decreases with temperature (within an interval of temperatures smaller than 100 K), and (iii) d practically vanishes at higher temperatures. The interval of pronounced changes in d is characterized by the depolymerization temperature T_{depol} that describes the life-time of a polymer and equals the temperature at which the mass loss reaches 5 %.

In GPA tests with a constant temperature T , a specimen is rapidly heated to the required temperature, which remains constant during the experimental procedure, and the sample’s mass is measured as a function of exposure time t . The function $d(t)$ monotonically decreases from $d(0) = 1$ and tends to zero with the growth of exposure time t . The decrease in mass at a given temperature T is characterized by the half-life time t_{hl} that is determined as the exposure time at which the sample loses half of its initial mass.

To compare predictions of the model with the experimental data available in the literature, we perform numerical integration of Eqs. (33) and (35) with $K = 100$ and $\Delta t = 1.0 \cdot 10^{-3}$ [these values guarantee that the evolution of the first moments $M_m(t)$ ($m = 0, 1, 2$) is independent of the integration algorithm] for poly(α -methylstyrene) with $a = 0.0$, $b = 1.5$ and $\eta = 50.0$ (these values are found by matching the experimental data presented in Figure 9). The effect of temperature T on the rate of fragmentation γ_0 is described by Eqs. (44) and (45) with $\gamma_0^{\text{ref}} = 9.0 \cdot 10^{-7}$, $A_0 = 26.86$ and $A_1 = 10344.0$ (these values are determined by matching the observations depicted in Figure 10). To take into account the influence of the initial molecular

weight $M_w(0)$, we use Eq. (41) with $M_w^{\text{ref}}(0) = 9.0$ kg/mol. The ratio of the current mass $\bar{m}(t)$ to the initial mass $\bar{m}(0)$ is determined by Eq. (31), where the moment $M_1(t)$ is given by Eq. (12).

Integration of Eq. (35) is carried out for $M_w(0) = 4.0$ kg/mol and $M_w = 680.0$ kg/mol (in the latter case, a correction factor of 1.5 is introduced in Eq. (41) in accord with the experimental data reported in Figure 3 of [32]) for the first kind of thermo-gravimetric tests with $q = 10.0$ K/min and for $M_w = 680.0$ kg/mol for the other kind of experiments at the temperature $T = 560$ K. The results of numerical analysis are presented in Figures 13 and 14. These figures demonstrate that the shapes of the curves $d(T)$ and $d(t)$ are similar to those reported in numerous experimental studies.

To show that our results of numerical simulation provide quantitative coincidence with observations, we depict (in Figure 13) the onset temperature T_{onset} for degradation of PAMS with the low molecular weight $M_w(0) = 4.0$ kg/mol [35], and the depolymerization temperature T_{depol} for PAMS with the high molecular weight $M_w = 680.0$ kg/mol [36]. For the same purpose, we plot the boundaries of the interval for the half-life time t_{hl} of PAMS at $T = 560$ K reported in [36]. Striking similarity is observed between the experimental data and the model predictions.

8 Conclusions

A kinetic model is analyzed for thermal degradation of polymers. The governing relations are based on the fragmentation–annihilation concept. According to this approach, thermal degradation reflects two processes at the micro-level: (i) binary fragmentation of macromolecules and (ii) scission of end- and side-groups and their annihilation (diffusion and evaporation) from the network of chains. The evolution equations involve four material constants that are determined by fitting experimental data for polystyrene, poly(α -methylstyrene) and poly(L-lactide).

Two explicit solutions of the integro-differential equations are found by using the method of generating function and the Charlesby method. These solutions (corresponding to special values of adjustable parameters) serve as a basis for numerical analysis. Numerical simulation of the kinetic equations is performed to study the effect of material constants on the evolution of mass-average and number-average molecular weights of polymers with exposure time.

With reference to available experimental data, two superposition principles (time–temperature and time–molecular weight) are formulated, and restrictions on material constants are found that guarantee their validity. These limitations allow the number of adjustable parameters to be reduced in order to make the approximation of observations more reliable.

It is revealed that the fragmentation–annihilation concept not only can be applied to describe experimental data on changes in the molecular weight, but can also be used to predict (qualitatively, and in some cases quantitatively) the mass decrease observed in TGA tests.

The following conclusions may be drawn from our analysis of experimental data on PS, PAMS and PLLA:

- The conventional assumption about the effect of chains' length ($a > 0$) on the fragmentation process is excessive. It results in a noticeable complication of the theoretical analysis, but does not improve the quality of fitting.
- The account of the influence of chains' length on the rate of annihilation is essential. The

parameter b weakly affects changes in the molecular weight with time at $b \in (0, 1)$, but its effect becomes important at higher values of the exponent b .

- The kinetics of polymer degradation is noticeably affected by the annihilation process when two conditions are fulfilled: (i) the number of end- and side-groups in polymer chains is rather large, and (ii) the rate of annihilation exceeds the rate of fragmentation of chains by (at least) an order of magnitude. Our results of numerical simulation demonstrate that the latter condition is satisfied at relatively high temperatures.

Appendix

The aim of this section is to derive an explicit formula for the evolution of the second moment M_2 with time t , when the fragmentation process is described by the conventional equation

$$\frac{\partial n}{\partial t}(t, x) = -\gamma_0 n(t, x) + 2\gamma_0 \int_x^\infty n(t, y) dy \quad (\text{A-1})$$

with an arbitrary initial condition (11). Equation (A-1) coincides with Eq. (11) where the annihilation process is disregarded ($\Gamma_0 = 0$). The derivation is presented as an appendix, because we use a conventional approach (the method of generating functions) for the study of Eq. (A-1). To the best of our knowledge, the final result is, however, novel.

We begin with the analysis of the moments $M_0(t)$ and $M_1(t)$. It follows from Eq. (15) that these functions are governed by the differential equation

$$\frac{dM_0}{dt}(t) = \gamma_0 M_1(t), \quad \frac{dM_1}{dt}(t) = 0. \quad (\text{A-2})$$

Integrating Eq. (A-2) and bearing in mind that

$$M_0(0) = 1$$

[this equality follows from Eqs. (1), (8) and (12)], we obtain

$$M_0(t) = 1 + \gamma_0 M_1(0)t, \quad M_1(t) = M_1(0). \quad (\text{A-3})$$

We now multiply Eq. (A-1) by $\exp(-zx)$, where z is a new variable, and integrate the result over x from zero to infinity. Introducing the notation [the Laplace transform of the function $n(t, x)$]

$$\hat{n}(t, z) = \int_0^\infty n(t, x) \exp(-zx) dx, \quad (\text{A-4})$$

we find that

$$\frac{\partial \hat{n}}{\partial t}(t, z) = -\gamma_0 \int_0^\infty x n(t, x) \exp(-zx) dx + 2\gamma_0 \int_0^\infty \exp(-zx) dx \int_x^\infty n(t, y) dy. \quad (\text{A-5})$$

According to Eq. (A-4), the first integral on the right-hand side of Eq. (A-5) reads

$$\int_0^\infty x n(t, x) \exp(-zx) dx = -\frac{\partial \hat{n}}{\partial z}(t, z).$$

To transform the other integral, we change the order of integration and use Eqs. (12) and (A-4),

$$\begin{aligned} \int_0^\infty \exp(-zx) dx \int_x^\infty n(t, y) dy &= \int_0^\infty n(t, y) dy \int_0^y \exp(-zx) dx \\ &= \frac{1}{z} \int_0^\infty [1 - \exp(-zy)] n(t, y) dy = \frac{1}{z} [M_0(t) - \hat{n}(t, z)]. \end{aligned}$$

Substitution of these expressions into Eq. (A-5) results in the partial differential equation

$$\frac{\partial \hat{n}}{\partial t}(t, z) = \gamma_0 \frac{\partial \hat{n}}{\partial z}(t, z) + \frac{2\gamma_0}{z} [M_0(t) - \hat{n}(t, z)]. \quad (\text{A-6})$$

Introducing the function

$$\Phi(t, z) = \hat{n}(t, z) - M_0(t), \quad (\text{A-7})$$

we present Eq. (A-6) in the form

$$\frac{\partial \Phi}{\partial t}(t, z) + \frac{dM_0}{dt}(t) = \gamma_0 \frac{\partial \Phi}{\partial z}(t, z) - \frac{2\gamma}{z} \Phi(t, z).$$

It follows from this equality and Eq. (A-2) that

$$\frac{\partial \Phi}{\partial t}(t, z) - \gamma_0 \frac{\partial \Phi}{\partial z}(t, z) = -\frac{2\gamma_0}{z} \Phi(t, z) - \gamma_0 M_1(0). \quad (\text{A-8})$$

We search a solution of Eq. (A-8) in the form $\Phi = \Psi(x_1, x_2)$, where

$$x_1 = t + \frac{z}{\gamma_0}, \quad x_2 = z. \quad (\text{A-9})$$

In the new notation, Eq. (A-8) reads

$$\frac{\partial \Psi}{\partial x_2}(x_1, x_2) = M_1(0) + \frac{2}{x_2} \Psi(x_1, x_2). \quad (\text{A-10})$$

An advantage of Eq. (A-10) is that it includes x_1 as a parameter. We now introduce the function $\Psi_1(x_1, x_2)$ by the formula

$$\Psi(x_1, x_2) = x_2^2 \Psi_1(x_1, x_2). \quad (\text{A-11})$$

Equations (A-10) and (A-11) imply that this function satisfies the equation

$$\frac{\partial \Psi_1}{\partial x_2}(x_1, x_2) = \frac{M_1(0)}{x_2^2}. \quad (\text{A-12})$$

The general solution of Eq. (A-12) reads

$$\Psi_1(x_1, x_2) = -\frac{M_1(0)}{x_2} + F(x_1),$$

where F is an arbitrary smooth function of x_1 . Returning to the initial notation with the help of Eqs. (A-7), (A-9) and (A-11), we obtain

$$\hat{n}(t, z) = M_0(t) - M_1(0)z + F\left(t + \frac{z}{\gamma_0}\right)z^2. \quad (\text{A-13})$$

It follows from Eqs. (11) and (A-4) that

$$\hat{n}(0, z) = \hat{n}_0(z), \quad \hat{n}_0(z) = \int_0^\infty \exp(-zx)n_0(x)dx. \quad (\text{A-14})$$

Setting $t = 0$ in Eq. (A-13) and using Eq. (A-14), we find that

$$F(z) = \frac{1}{(\gamma_0 z)^2} [\hat{n}_0(\gamma_0 z) - M_0(0) + M_1(0)\gamma_0 z]. \quad (\text{A-15})$$

Equations (12) and (A-4) imply that

$$M_2(t) = \frac{\partial^2 \hat{n}}{\partial z^2}(t, 0). \quad (\text{A-16})$$

Differentiation of Eq. (A-13) with respect to z results in

$$\frac{\partial^2 \hat{n}}{\partial z^2}(t, 0) = 2F(t).$$

Combining this equality with Eqs. (A-15) and (A-16), we arrive at the formula

$$M_2(t) = \frac{2}{(\gamma_0 t)^2} [\hat{n}_0(\gamma_0 t) - M_0(0) + M_1(0)\gamma_0 t]. \quad (\text{A-17})$$

Equations (A-3) and (A-17) provide explicit formulas for the evolution of three first moments M_m driven by thermal degradation of a polymer with an arbitrary initial distribution of chain lengths.

References

- [1] Grassie N and Scott G 1985 *Polymer Degradation and Stabilisation* (Cambridge: Cambridge Univ. Press)
- [2] Allen NS and Edge M 1992 *Fundamentals of Polymer Degradation and Stabilization* (New York: Elsevier).
- [3] Rangarajan P, Bhattacharyya D and Grulke E 1998 *J. Appl. Polym. Sci.* **70**, 1239–51
- [4] Ziff RM and McGrady ED 1985 *J. Phys. A: Math. Gen.* **18**, 3027–37
- [5] Ziff RM and McGrady ED 1986 *Macromolecules* **19**, 2513–9
- [6] Ernst MH and Szamel G 1993 *J. Phys. A: Math. Gen.* **26**, 6085–91
- [7] Singh P and Rodgers GJ 1995 *Phys. Rev. E* **51**, 3731–4
- [8] Tayal A and Khan SA 2000 *Macromolecules* **33**, 9488–93
- [9] Kostoglou M and Karabelas AJ 2001 *J. Phys. A: Math. Gen.* **34**, 1725–40
- [10] Chan JH and Balke ST 1997 *Polym. Degrad. Stab.* **57**, 113–25, 127–34, 135–49
- [11] Madras G, Chung GY, Smith JM and McCoy BJ 1997 *Ind. Eng. Chem. Res.* **36**, 2019–24
- [12] Kumar GS, Kumar VR and Madras G 2002 *J. Appl. Polym. Sci.* **84**, 681–90
- [13] Betso SR, Berdasco JA, Debney MF, Murphy GL, Rome NP, Richards SG and Howell BA 1994 *J. Appl. Polym. Sci.* **51**, 781–805
- [14] Boyer D, Tarjus G and Viot P 1995 *Phys. Rev. E* **51**, 1043–6
- [15] Verdu S and Verdu J 1997 *Macromolecules* **30**, 2262–7
- [16] Sterling WJ, Kim Y-C and McCoy BJ 2001 *Ind. Eng. Chem. Res.* **40**, 1811–21
- [17] Karmore V and Madras G 2002 *Ind. Eng. Chem. Res.* **41**, 657–60
- [18] Medhekar V, Thompson RW, Wang A and McGimpsey WG 2003 *J. Appl. Polym. Sci.* **87**, 814–26
- [19] Costas ME, Moreau M and Vicente L 1995 *J. Phys. A: Math. Gen.* **28**, 2981–94
- [20] Jeffrey GC and Ottewill RH 1990 *Colloid Polym. Sci.* **268**, 179–89
- [21] Laurenzi IJ and Diamond SL 2003 *Phys. Rev. E* **67**, 051103
- [22] Yu H, Huang N, Wang C and Tang Z 2003 *J. Appl. Polym. Sci.* **88**, 2557–62
- [23] Ben-Naim E and Krapivsky PL 1995 *Phys. Rev. E* **52**, 6066–70
- [24] Filipe JAN and Rodgers GJ 1996 *Phys. Rev. E* **54**, 1290–7

- [25] Krapivsky PL and Ben-Naim E 2000 *J. Phys. A: Math. Gen.* **33**, 5465–75
- [26] Edwards BF, Cai M and Han H 1990 *Phys. Rev. A* **41**, 5755–7
- [27] Huang J, Edwards BF and Levine AD 1991 *J. Phys. A: Math. Gen.* **24**, 3967–77
- [28] Singh P and Rodgers GJ 1996 *J. Phys. A: Math. Gen.* **29**, 437–50
- [29] Elhanbaly A 2003 *J. Phys. A: Math. Gen.* **36**, 8311–23
- [30] Charlesby A 1954 *Proc. Roy. Soc. London A* **224**, 120
- [31] Ferry JD 1980 *Viscoelastic Properties of Polymers* (New York: Wiley)
- [32] Bywater S and Black PE 1965 *J. Phys. Chem.* **69**, 2967–70
- [33] Brown DW and Wall LA 1958 *J. Phys. Chem.* **62**, 848–52
- [34] Eyring H 1936 *J. Chem. Phys.* **4**, 283–91
- [35] Burkey DD and Gleason KK 2003 *Chem. Vap. Deposition* **9**, 65–71
- [36] Kane L and Spontak RJ 1999 In: Mark JE (Ed.) *Polymer Data Handbook* (New York: Oxford Univ. Press) pp. 680–87

List of figures

- Figure 1:** The ratio of number-average molecular weights d_n versus dimensionless time t . Curves: results of numerical simulation for $a = 0.0$, $b = 1.0$ and $\eta = 0.0, 1.0, 10.0, 100.0$ and 200.0 , from top to bottom, respectively
- Figure 2:** The ratio of mass-average molecular weights d_w versus dimensionless time t . Curves: results of numerical simulation for $a = 0.0$, $b = 1.0$ and $\eta = 0.0, 1.0, 10.0, 100.0$ and 200.0 , from top to bottom, respectively
- Figure 3:** The ratio of number-average molecular weights d_n versus dimensionless time t . Curves: results of numerical simulation for $b = 1.0$, $\eta = 10.0$ and $a = 0.3, 0.6, 0.9$ and 1.2 , from top to bottom, respectively
- Figure 4:** The ratio of mass-average molecular weights d_w versus dimensionless time t . Curves: results of numerical simulation for $b = 1.0$, $\eta = 10.0$ and $a = 0.3, 0.6, 0.9$ and 1.2 , from top to bottom, respectively
- Figure 5:** The ratio of number-average molecular weights d_n versus dimensionless time t . Curves: results of numerical simulation for $a = 0.2$, $\eta = 10.0$ and $b = 0.0, 1.0, 1.5, 2.0$ and 2.5 , from top to bottom, respectively
- Figure 6:** The ratio of mass-average molecular weights d_w versus dimensionless time t . Curves: results of numerical simulation for $a = 0.2$, $\eta = 10.0$ and $b = 0.0, 1.0, 1.5, 2.0$ and 2.5 , from top to bottom, respectively
- Figure 7:** The ratio of mass-average molecular weights d_w versus time t min. Symbols: treatment of observations on PS with the initial molecular weights $M_w(0) = 26$ (triangles), 110 (stars), 210 (asterisks), 330 (filled circles) and 930 kg/mol (unfilled circles). Solid line: results of numerical simulation
- Figure 8:** The shift factor A versus the ratio of mass-average molecular weights. Circles: treatment of observations on PS. Solid line: approximation of the experimental data by Eq. (40) with $A_0 = 0.05$ and $A_1 = 0.83$
- Figure 9:** The ratio of number-average molecular weights d_n versus time t . Symbols: treatment of observations on PAMS at the temperatures $T = 110$ (unfilled circles), $T = 120$ (filled circles), $T = 130$ (asterisks), $T = 140$ (stars) and $T = 150$ °C (diamonds). Solid line: results of numerical simulation
- Figure 10:** The shift factor A versus temperature T . Circles: treatment of observations on PAMS. Solid line: approximation of the experimental data by Eq. (44) with $A_0 = 26.86$ and $A_1 = 1.03 \cdot 10^4$
- Figure 11:** The ratio of number-average molecular weights d_n versus time t . Symbols: experimental data on PLLA. Solid lines: results of numerical simulation

Figure 12: The shift factors A (unfilled circles) and B (filled circles) versus temperature T . Circles: treatment of observations on PLLA. Solid lines: approximation of the experimental data by Eq. (47). Curve 1: $A_0 = 24.53$, $A_1 = 1.11 \cdot 10^4$. Curve 2: $B_0 = 59.90$, $B_1 = 2.69 \cdot 10^4$

Figure 13: The ratio d of a sample's mass to its initial mass versus temperature T . Solid lines: results of numerical simulation for PAMS under heating with the rate $q = 10.0$ K/min. Curve 1: $M_w(0) = 4.0$ kg/mol. Curve 2: $M_w(0) = 680.0$ kg/mol. Vertical lines: the onset temperature T_{onset} for thermal degradation of the low-molecular weight PAMS and the depolymerization temperature T_{depol} for the high-molecular weight PAMS

Figure 14: The ratio d of a sample's mass to its initial mass versus exposure time t at the temperature $T = 560$ K. Solid line: results of numerical simulation for PAMS. Vertical lines denote the interval of time where a specimen loses a half of its initial mass

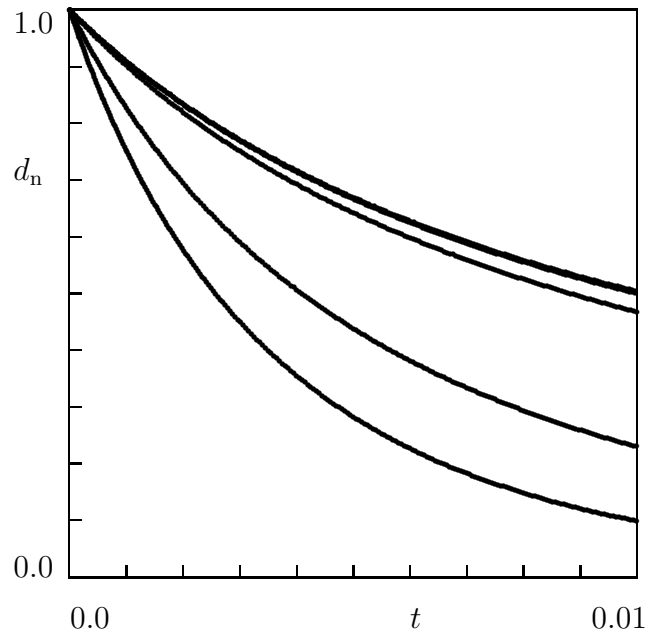


Figure 1:

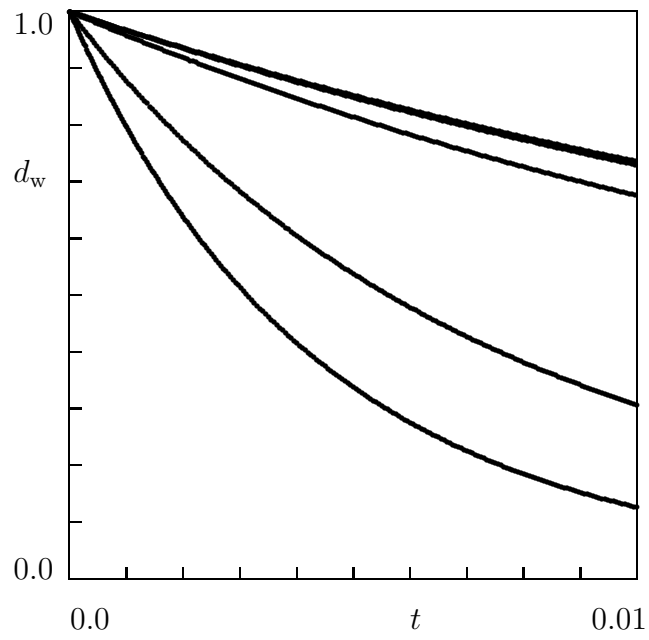


Figure 2:

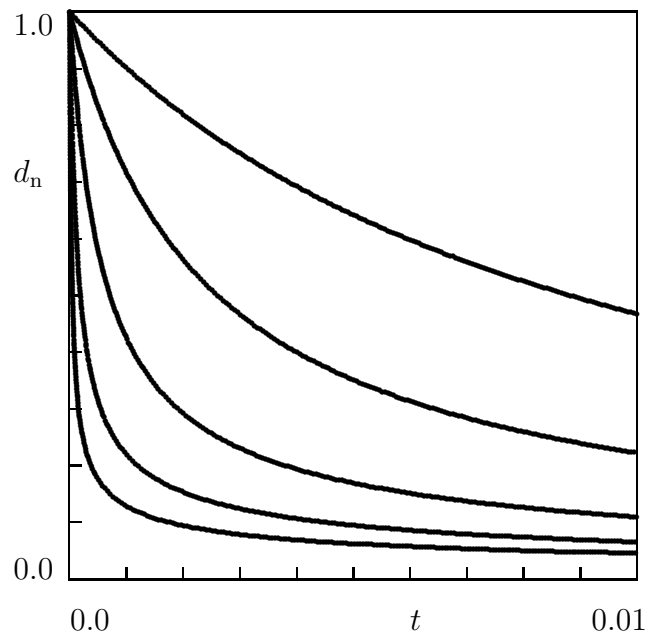


Figure 3:

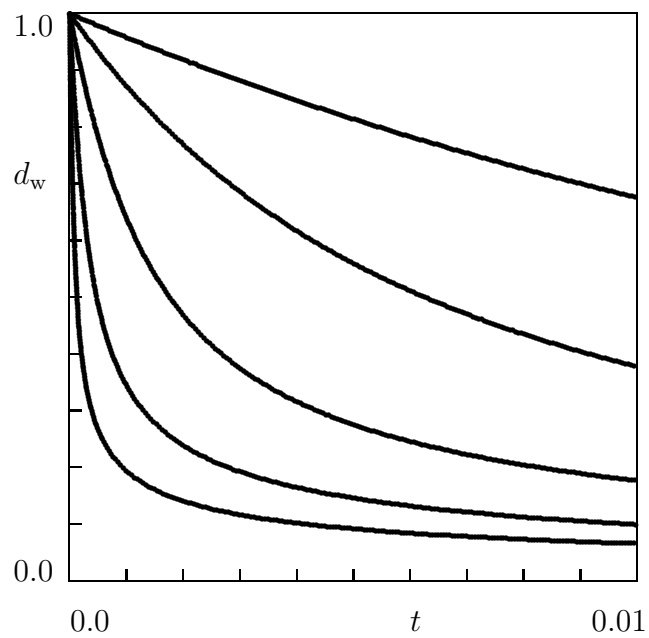


Figure 4:

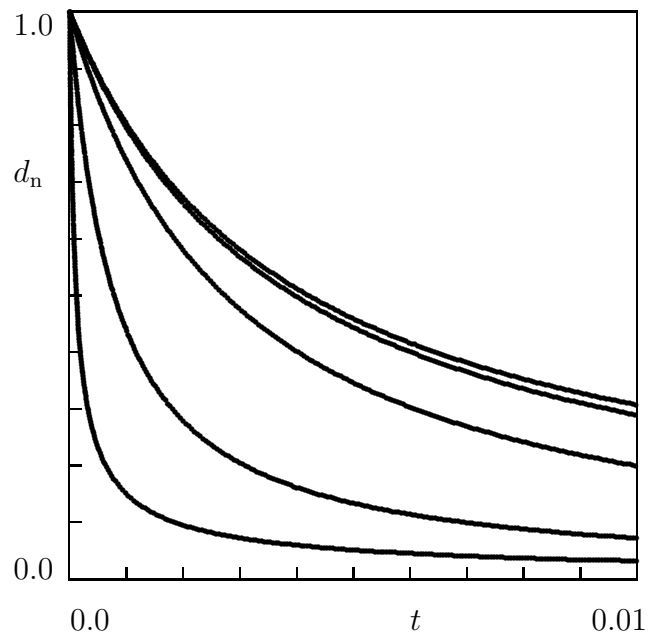


Figure 5:

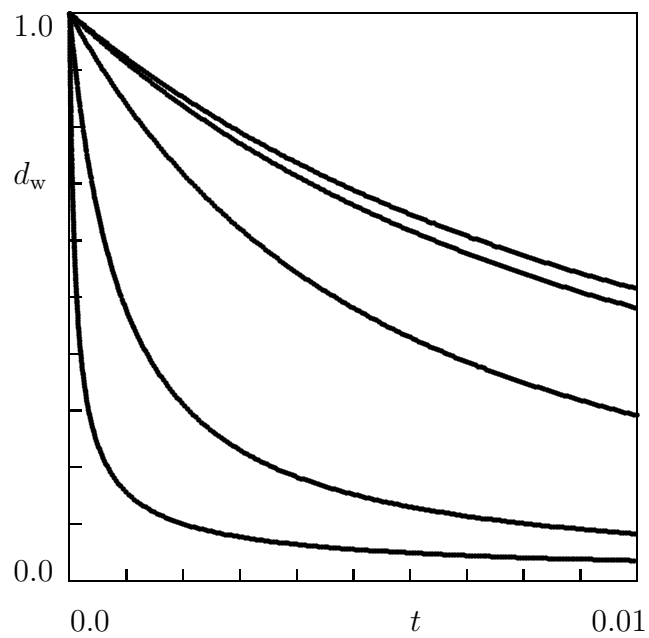


Figure 6:

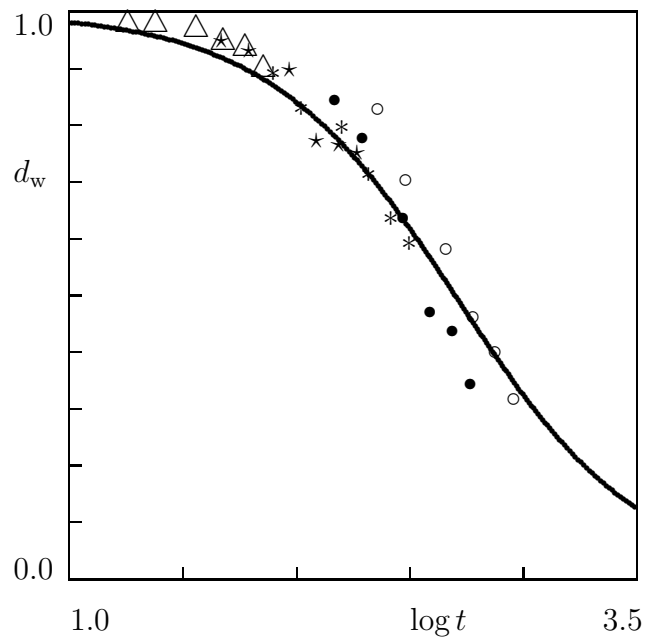


Figure 7:

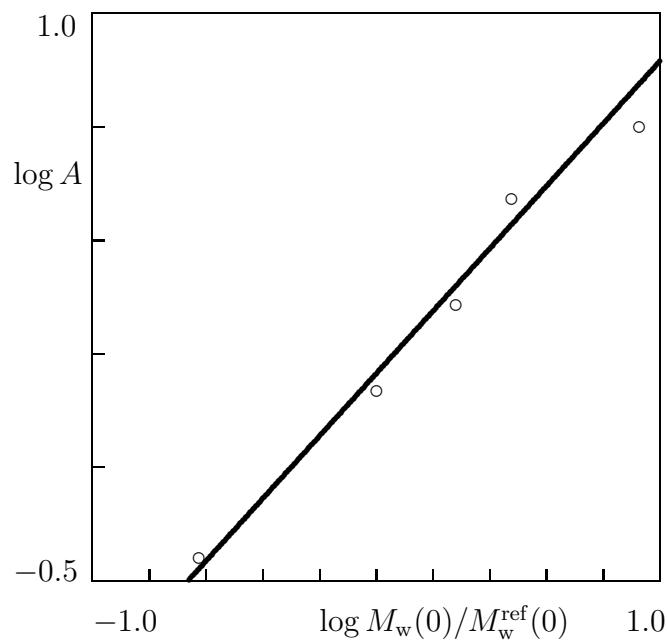


Figure 8:

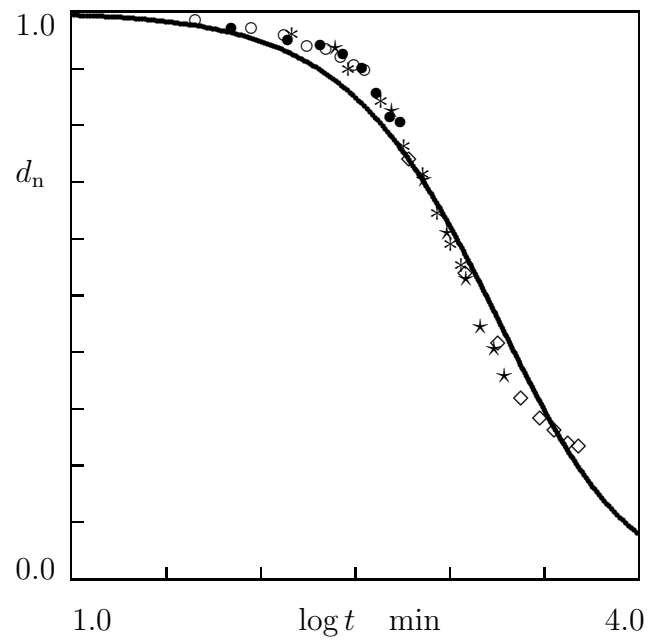


Figure 9:

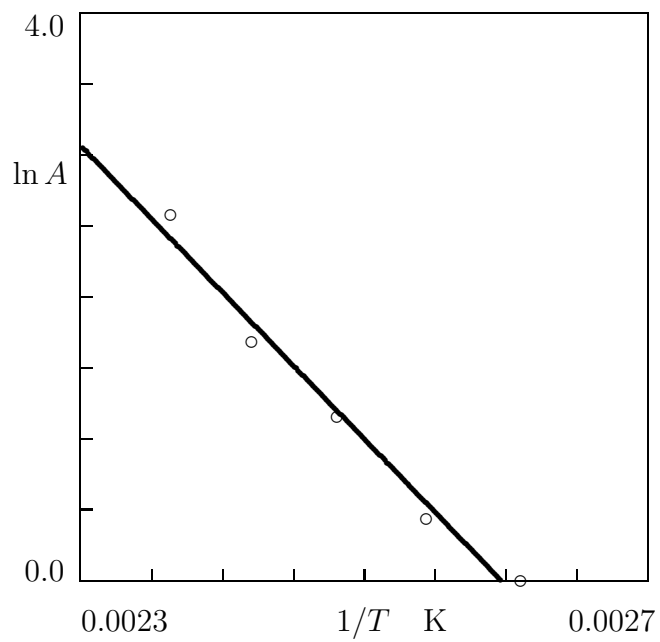


Figure 10:

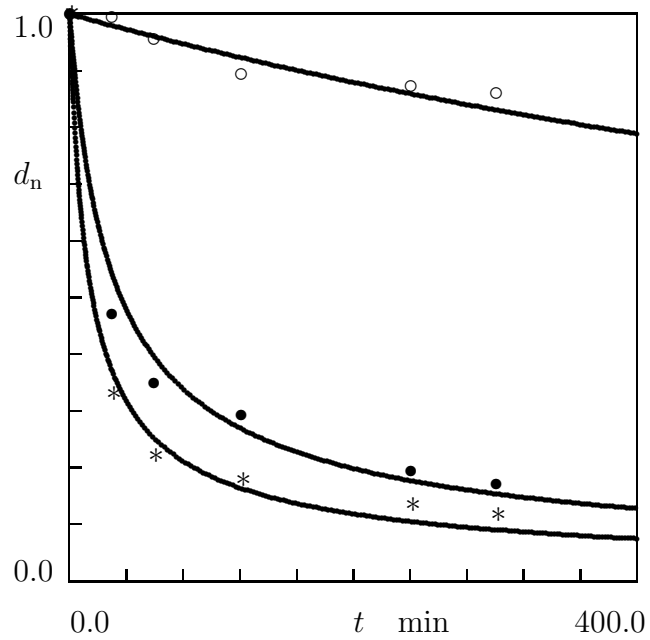


Figure 11:

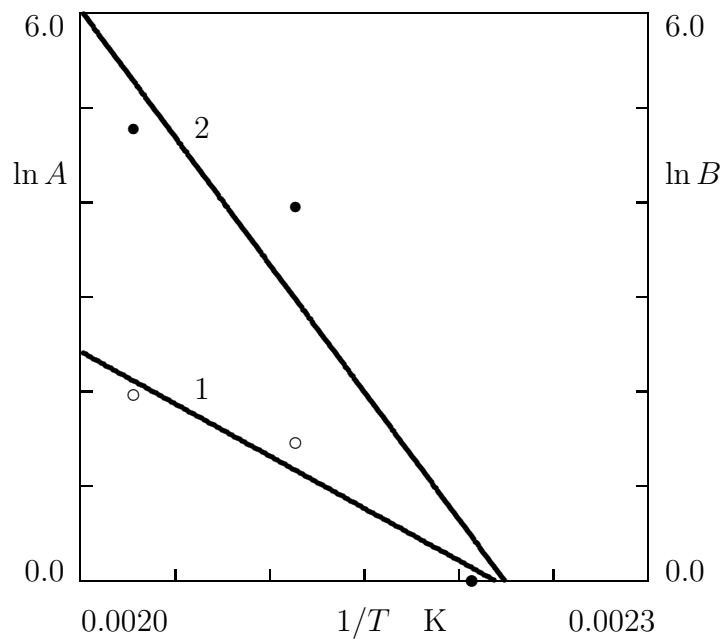


Figure 12:

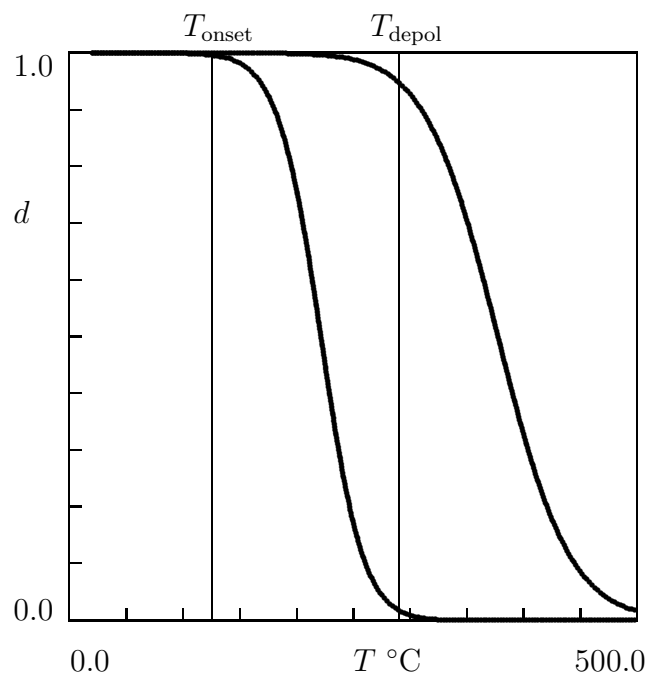


Figure 13:

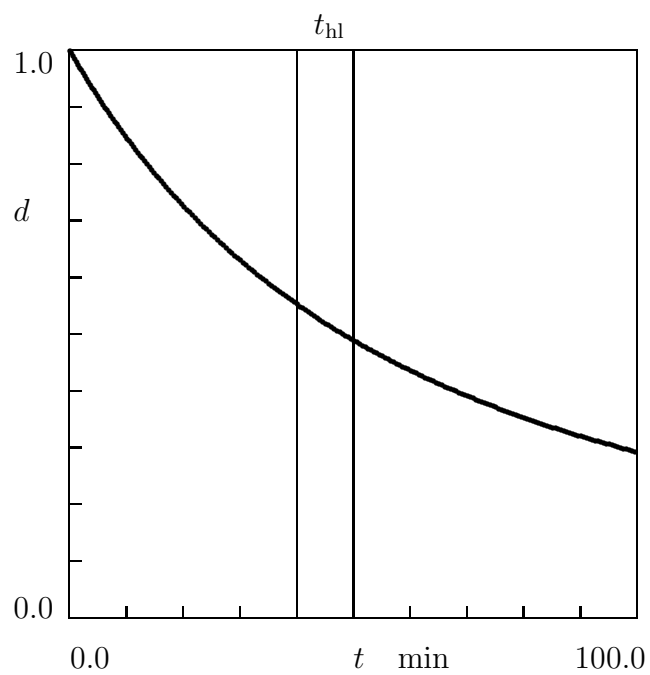


Figure 14: